Title: Surface modification of TiO_2 with copper clusters for band gap narrowing

Authors: Preetam K. Sharma, Maria Ana L.R.M. Cortes, Jeremy W.J. Hamilton, Yisong Han, J. Anthony Byrne, Michael Nolan

PII: S0920-5861(17)30821-0
DOI: https://doi.org/10.1016/j.cattod.2017.12.002
Reference: CATTOD 11154

To appear in: *Catalysis Today*

Received date: 28-7-2017
Revised date: 8-11-2017
Accepted date: 5-12-2017

Please cite this article as: Preetam K.Sharma, Maria Ana L.R.M.Cortes, Jeremy W.J.Hamilton, Yisong Han, J.Anthony Byrne, Michael Nolan, Surface modification of TiO2 with copper clusters for band gap narrowing, Catalysis Today https://doi.org/10.1016/j.cattod.2017.12.002

Surface modification of TiO_2 with copper clusters for band gap narrowing

Preetam K. Sharma[a,*], Maria Ana L. R. M. Cortes[a], Jeremy W. J. Hamilton[a], Yisong Han[a], J. Anthony Byrne[a], Michael Nolan[b]

***Corresponding author:** pk.sharma@ulster.ac.uk

[a] NIBEC, Ulster University, Shore Road, Newtownabbey, BT37 0QB, United Kingdom

[b] Tyndall National Institute, Lee Maltings, University College Cork, Dyke Parade, T12 R5CP, Cork, Ireland

Graphical Abstract

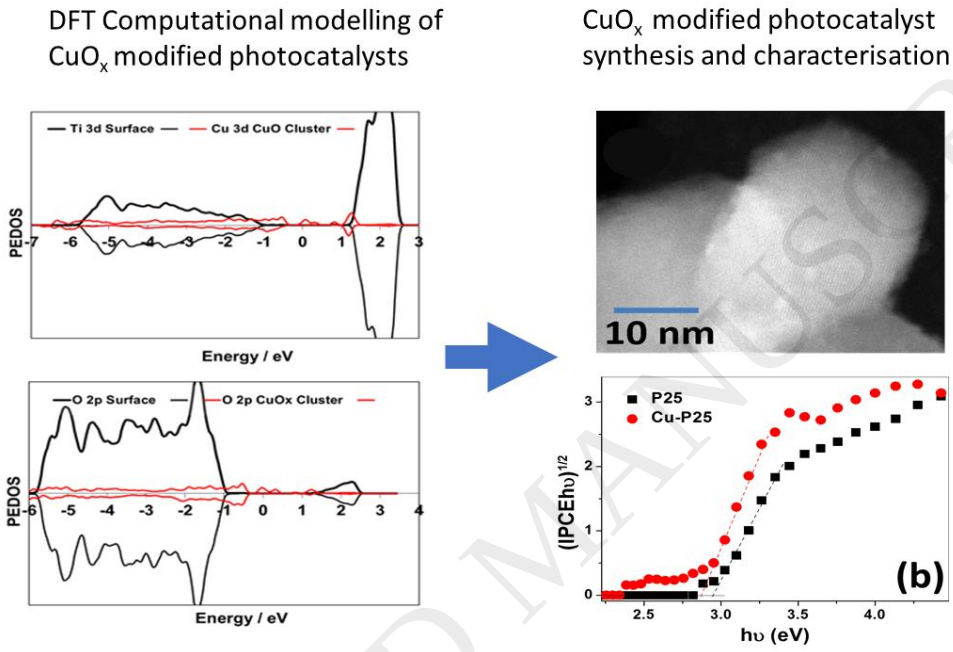

Research highlights

- Successful computational design to discover new photocatalytic materials that may be useful for solar applications
- CuO & CuO_x molecular cluster modified TiO_2 photocatalysts where investigated by DFT modelling
- Modelling predicted Cu states within the band gap of TiO_2 for both CuO & CuOx surface modifying molecular clusters
- Physical Characterisation of the CuO_x modified TiO_2 showed a red shift in optical adsorption and valence band XPS.
- Photoelectrochemical characterisation, showed an increase and a small red shift in the IPCE for CuOx modified TiO_2 compared to TiO_2.

Abstract

Surface modification of photocatalytic materials to give better activity, and potentially extending the response into the visible spectrum, is an area of active research. In this work, DFT modelling suggests that surface modification of rutile and anatase TiO_2 with partially oxidised copper clusters can induce a red shift in the photo-action spectrum. Copper clusters were synthesised and characterised separately before TiO_2 nanoparticle surface modification.

Characterisation of copper clusters and photocatalysts modified with copper clusters showed that ex-situ synthesis can control the size of surface clusters. Sub-nanometre clusters of copper maintained their size and morphology upon attachment to the photocatalyst surface. The copper clusters we determined to be a mixture of Cu(0) and Cu(I), and no significant change in the oxidation state was observed following surface modification or following photoelectrochemical measurements. Experimental measurements including UV-Vis spectroscopy and valence band XPS showed a small red shift the band gap correlating to the DFT predictions. Photoelectrochemical characterisation showed an enhancement in the UV photocurrent response and a small red shift in the effective band gap for the surface modified TiO_2.

Keywords: TiO_2; copper clusters; surface modification; band gap engineering; DFT modelling; X-ray photoelectron spectroscopy; photoelectrochemical water splitting

1 Introduction

The conversion of solar energy to chemical energy by photocatalytic water splitting or carbon dioxide reduction could potentially help reduce carbon emissions and provide improved security of energy supply. Efficient solar photocatalysis requires a stable and preferably inexpensive material which has absorption in both UV and visible region [1]. Titanium dioxide has a band gap of 3.2 eV for anatase which requires UV excitation [2, 3]. Extending the photoactivity spectrum of TiO_2 into the visible region of the solar spectrum by doping with metals and non-metals has had limited success due to doping induced defects which act as recombination centres [4].

The surface modification of titanium dioxide nanomaterials with metals, metal oxides and sulphides has been reported to give a red shift in the photoresponse spectrum. The decoration of TiO_2 surface with metal sulphides like CdS and ZnS has been reported to give strong changes in the optical absorption with size-dependant behaviour [5]. However, metal sulphides are not stable in aqueous environments and can undergo photocorrosion [6]. To realize size dependent band gap modification, alternative materials based on metals or metal oxides as molecular clusters represent a more stable choice of surface modifier. Surface modification with plasmonic metal nanoparticles such as gold or platinum, which are resistant to oxidation, have been reported to give an increase in photocatalytic activity through a plasmon induced surface sensitisation mechanism [7,8]. To truly extend the activity spectrum of a photocatalyst, surface modifications should alter the parent material by bonding directly to the lattice creating new energy levels distinct from either material. Combined modelling and experimental evidence has reported that modification with sub-nanometre surface-bound metal oxide clusters can extend the valence band of TiO_2 by formation of interfacial bonds which induce new electronic states in the energy gap. [9] . This was demonstrated for the examples of NiO [10] and SnO [11] modified rutile and anatase TiO_2 by the upshift of the

valence band edge due to new oxide cluster derived states. Modelling has been successfully used to predict the nature and oxidation states of the oxide cluster modifier [9, 12, 13], the red shift [9, 12,13] and the reactivity of the composite material [14,15].

In addition to modulating band edge potentials, through disruption of the lattice order, surface species can act as trapping sites for photogenerated charges [16,17]. Localisation of photogenerated electrons into these surface clusters allows the chemical nature of the surface cluster to then influence electrochemical reduction and hence product distributions. By considering photocatalyst modification with molecular clusters and charge localisation at a co-catalyst site, [18, 19] these surface modifiers can be considered to behave like electrocatalysts. Metallic Cu(0) clusters can scavenge VB holes and provide an alternative charge separation pathway [20]. Cu(0) can also inject charges into the CB of TiO_2 via localized surface plasmon resonance [25,21]. Cu_2O is a p-type semiconductor with a bandgap of 2.1 eV with appropriate band-edge potentials for water splitting [22]. However, Cu_2O is not an appropriate photocatalyst on its own due photo-corrosion [23]. Wang et al. have shown that Cu_2O is the active species for TiO_2 surface modification for H_2 production [24]. In a similar study, electrodeposited Cu_2O on TiO_2 has been shown to split water efficiently [25]. Predominantly, Cu_2O has been reported as the active species in reducing electron-hole pair recombination and as an active site for multi-electron transfers. Wang et al. have shown that Cu-TiO_2 nanomaterials, produced by the reaction of Cu(I) salts, photoreduced to Cu(0) and re-oxidized in ambient conditions, can work as stable photocatalysts if the formation of the CuO is avoided [26]. Theoretical investigations have shown that the presence of low co-ordinated Cu on the surface can induce a shift in the valence band edge mainly via the sub-band gap states of Cu 3d [27]. Additionally, the formation of Cu-Ti bonds and Ti^{3+} can influence the electrical and properties of the material through these mid-gap states inducing alternative conduction paths. These mid bandgap states might enhance the photocatalytic activity of TiO_2 by absorbing photons and/or enhancing electron-hole pair separation [28].

In this work, we present DFT modelling to examine the atomic level details of surface modification of TiO_2 with Cu clusters, focussing on the preferred state of the surface bound clusters and any red shift in light absorption. In experimental work, the Cu clusters were prepared separately using a wet chemical method, and then used to modify the surface of TiO_2. We find band gap narrowing can be observed by a number of experimental techniques, however the extent of the red shift and enhancement of photocurrent response were limited following copper modification. The agreement between DFT and experiment provides new insights into the nature and properties of copper cluster modified TiO_2.

2 Experimental Section

2.1 DFT modelling of copper oxide modified TiO_2

DFT calculations were performed within three dimensional periodic boundary conditions with a plane wave basis set to describe the valence electron wavefunctions, implemented in VASP5.2 [29,30]. The details of the methodology are given in the supplementary section S1.

2.2 Synthesis of copper molecular clusters

Copper molecular clusters were synthesized by adopting modified Brust-Schiffrin protocol [31]. Copper (II) nitrate trihydrate (4 mM, $Cu(NO_3)_2 \cdot 3H_2O$, Sigma Aldrich) and 10 mM of tetra-n-octylammonium bromide (TOAB, Alfa Aesar) were dissolved in absolute ethanol (Sigma Aldrich) under constant stirring to obtain a dark green solution. The solution was kept at 80°C for 30 min followed by cooling in ice water. The solution was then sparged with Ar gas followed by addition of 20 mM of 2-mercapto-5-n-propylpyrimidine (MPP, Alfa Aesar). The solution was left to react over-night under constant stirring and Ar sparging. Sodium borohydride (50 mM, Sigma Aldrich) in ethanol was then added into the reaction mixture. The reaction was stopped after 7 h giving a dark-yellow solution. Solutions were centrifuged at 12000 rpm, for 20 min to recover the Cu clusters, followed by multiple washing and centrifugation using ethanol as the solvent. The washed pellet was vacuum dried at room temperature. The mechanism of Cu cluster formation and stabilisation are described in the supplementary section S2.

2.3 Surface modification of TiO_2

TiO_2 (P25, Evonik Aeroxide) was mixed with copper clusters (2 wt% Cu to TiO_2) in methanol followed by sonication. A suspension of TiO_2 (1 wt%) with or without Cu) was used to spray coat Ti foil from a lab spray gun [32]. Before coating, the 20 x 25 mm^2 Ti foils were cleaned by sonicating for 15 min in detergent solution, followed by multiple washing in distilled water. The foils were dried under an Ar stream. Following spray coating, the TiO_2 (with or without Cu modification) loading on foil was 1 mg cm^{-2}. The samples were then annealed at 550^{o}C for 1 h in air to provide particle cohesion and adhesion to the foil (ramp 2^{o}C min^{-1} up, 1^{o}C min^{-1} down). This annealing temperature was selected based on weight loss profiles determined by TGA showing ligand oxidation at 547^{o}C (data not shown). To form electrodes, an uncoated area of Ti foil was cleaned using abrasive paper, and a Cu wire was connected to the foil using conductive silver epoxy (CircuitWorks CW2400). Any area of the electrode not coated with TiO_2 was insulated using SU-8 photoresist (MicroChem) leaving an active area of 20 x 20 mm^2. The SU-8 coated samples were exposed to UVB for 5 min on both sides, to cross link the photoresist, followed by hard baking at 160°C.

2.4 Photoelectrochemisty

Potentiostatic control was implemented using an Autolab PG30 electrochemical workstation. The irradiation source was a 450 W Xe lamp. For monochromatic irradiation, a Horiba Jobin Yvonne microHR monochromator was used. A Uniblitz chopper was used for chopped irradiation experiments. For visible only polychromatic irradiation, a 435 nm cut off filter was

used. Electrochemical measurements were performed in 0.1 M $HClO_4$ as a backing electrolyte in a three-electrode configuration with a Pt gauze counter electrode and a saturated calomel reference electrode. All potentials are reported relative to SCE. Linear sweep voltammetry was used to measure the current-potential response under polychromatic irradiation (full spectrum or visible $\lambda > 435$nm). The sweep rate was 5 mV s^{-1}, starting at -1.0 V up to +1.0 V. The spectral photocurrent response was measured at a fixed potential (+1.0 V), under monochromatic irradiation at 10 nm intervals (band pass FWHM 10 nm).

2.5 Materials characterisation

A Kratos Axis Ultra system was used to measure X-ray photoelectron spectra (XPS) from synthesised catalysts, with 284.8 eV used for calibration of C 1s chemical shifts. The data was fitted using mixed Gaussian-Lorentzian (GL30) on a Shirley background. The UV-Vis reflectance spectra were obtained on Perkin Elmer Labmda 35 spectrophotometer. The reflectance data was used to obtain the Kubelka-Munk function $(F(R)=(1-R)^2/2R)$ as a function of wavelength. The Kubelka-Munk function was used for the Tauc plot. Direct and indirect band gaps were determined by plotting $(F(R)h\upsilon)^2$ vs $h\upsilon$ and $(F(R)h\upsilon)^{1/2}$ vs $h\upsilon$. Transmission (TEM) and scanning transmission electron microscopic (STEM) images were recorded using Jeol JEM-2100F at 200 kV bias voltage. Scanning electron microscopy (SEM) was performed on a JEOL JSM-6010PLUS/LV at 20 kV. X-ray diffractograms (XRD) were recorded using Bruker D8 discover in 2θ range of 20 to 80 degrees.

3 Results and Discussion

3.1 Density Functional Theory modelling results

Figure 1 shows the atomic structure of perfect rutile (110) and anatase (101) surfaces modified with a Cu_4O_4 nanocluster (Figure 1(a), (c)) and a $Cu_{10}O_{10}$ nanocluster (Figure 1(e)). Upon adsorption, new cluster to surface bonds are formed between nanocluster copper and surface oxygen and surface titanium and nanocluster oxygen. The computed adsorption energies for these stoichiometric CuO nanoclusters are -7.45 eV on rutile (110) and -3.27/-2.41 eV for Cu_4O_4/$Cu_{10}O_{10}$ on anatase (101). These energies indicate strong adsorption of the CuO nanoclusters on both TiO_2 surfaces, arising from formation of the new nanocluster to surface bonds.

However, given the reducibility of supported oxide nanoclusters [14,15] we examine the stability of non-stoichiometric CuO through oxygen vacancy formation in supported CuO to produce CuO_x, with the atomic structures shown in Figures 1(b), (d), (f) and (g). For the supported Cu_4O_4 nanocluster, the formation energy of the most stable oxygen vacancy is +0.14 eV on rutile (110) and -0.51 eV on anatase (101). For the $Cu_{10}O_{10}$ nanocluster, the most stable oxygen vacancy has a computed formation energy of -0.02 eV, while the formation energy of the next oxygen vacancy, to give a $Cu_{10}O_8$ stoichiometry, is +0.06 eV. These

formation energies indicate that supported CuO nanoclusters are significantly non-stoichiometric

Upon formation of oxygen vacancies reduction of Cu cations takes place, with formation of two Cu^{+} species for each vacancy and no Ti reduction. The Cu^{+} species have a computed Bader atomic charge of 10.3 – 10.5 electrons, while Bader charges for Cu^{2+} species are 9.9-10.0 electrons. Cu^{+} cations have a spin of 0 ($3d^{10}$ configuration) and Cu^{2+} cations have a spin of 0.6 µB, consistent with results for bulk CuO [30,31].

The formation energy of the next oxygen vacancy, to give $Cu_{10}O_7$, is +1.24 eV so that a reducing oxygen vacancy can form and this vacancy reduces a further two Cu^{2+} cations to Cu^{+} (Bader charges of 10.4 electrons and a spin of 0); the atomic structure is shown in figure 1(g). Cu cations always reduce in preference Ti, so that the ground state of CuO-modified TiO_2 is a mixed Cu^{+}-Cu^{2+}oxide, denoted CuO_x. The experimental samples are annealed at 550^{o}C at which temperature further reduction of CuO_x is possible. Our work on CuO(111) shows that reduction of CuO ultimately leads to a mix of Cu^{0} and Cu^{+1}, consistent with the XPS data [31].

Figure 2(a) - (d) shows computed spin polarised projected electronic density of states (PEDOS) projected onto Cu 3d and Ti 3d states and the O 2p states in the nanocluster and support for Cu_4O_4-rutile (110), Cu_4O_4-anatase (101), $Cu_{10}O_{10}$-anatase (101) and $Cu_{10}O_8$-anatase (101). The PEDOS shows that the modification of both TiO_2 surfaces with CuO_x results in the introduction of CuO derived electronic states into the original valence to conduction band energy gap. The introduction of these CuO electronic states shifts the valence band edge to higher energy, which is investigated with valence band XPS, UV-Vis and spectral photocurrent measurements in the next section. We thus propose that CuO_x modified rutile or anatase will induce a red shift of the absorption edge of TiO_2, irrespective of the stoichiometry of the CuO nanocluster. We note that the DFT energy gap is underestimated, which is a well-known issue with approximate DFT functionals. However, our extensive work on surface modified TiO_2 [11,12,13,33] and experimental studies [10,34,35] have shown that despite this energy gap underestimation, the effect of the TiO_2 modification on the energy gap is well described, particularly the upshift of the valence band edge.

3.2 XPS analysis

Determination of the oxidation state of copper by XPS was performed by the examination of satellite peaks as there are only very small differences in the 2p peak position between the different oxidation states limiting the deconvolution strategies. The shift in Cu $2P_{3/2}$ peak position moving from Cu(0) to Cu(I) and Cu(II) equates to a shift of <1 eV in peak position with peaks expected at 932.61, 932.18 eV and 933.76 eV, respectively [36]. However, in the case of Cu(II) satellite peaks at 942 and 962 eV of equivalent height to the Cu $2P_{½}$ peak, expected

at 953 eV, are normally present [37]. As shown in figure 3(a) there are peaks at 932.4 and 952.2 eV corresponding to Cu $2P_{3/2}$ and $2P_{1/2}$, respectively. However, the absence of Cu(II) satellite peaks in the XPS analysis, suggests the copper clusters contain no Cu(II). To differentiate between metallic and +1 oxidation states, further investigation was performed in Auger electron spectral region corresponding to Copper LMM transition. The LMM transitions corresponding to metallic copper or copper oxide have peaks centred at 570 and 567.8 eV, separated by > 2 eV [38, 39]. As shown in figure 3(b), the molecular cluster has overlapping peaks at 570.2 and 568.0 eV corresponding to a mixed oxidation state of Cu(0) and Cu(I) oxide, respectively.

The Cu-P25 samples annealed at 550°C had very similar Cu 2p spectra to un-annealed Cu-TiO_2 samples (Figure S4). The absence of satellite peaks associated with Cu(II) in samples following annealing suggests that the oxidation state of the copper did not change significantly due to thermal treatment. The use of Cu LMM spectra could not provide information about further changes in the copper oxidation state due to the large Ti 2s background as shown in figure S5. The material did not significantly change its oxidation state and remained a mixture of Cu(0) and Cu(I) after loading onto the TiO_2 and annealing. We will continue to name the CuO_x modified TiO_2 as Cu-P25. Follow-up examination of the Cu 2p XPS region following photoelectrochemical measurements showed no marked changes in the spectra.

High resolution XPS for the P25 and Cu-P25 samples was carried out in the valence band region (Figure 3 (c)). The VB minima was shifted towards lower energy following copper loading. This shift consisted of a tail of additional states observed between 1 and ~3 eV. Discrimination between true band gap narrowing and a contribution from overlapping valence band edges in two distinct materials is not possible with this technique alone. However, there are various theoretical and experimental investigations of CuO_x on titania which support the presence of additional mid-gap states due to copper sub-d band [12]. The shift in the valence band edge observed in XPS equates to a reduction in bandgap of 0.62 eV.

3.4 STEM and EELS analysis

Figure 4 (a,b) shows the STEM images of the as prepared copper clusters. The STEM images were obtained at spot size of 0.2 nm, limiting the size of measurable particles to above this size. Figure 4(c) shows the particle size distribution of the clusters, with a mean particle size is ~ 8-9 Å. Electron energy loss spectroscopy (EELS) analysis was carried out to confirm the nature of particles. Due to the absence of oxygen peak at 531 eV, the particles were considered predominantly metallic copper, consistent with XPS measurements.

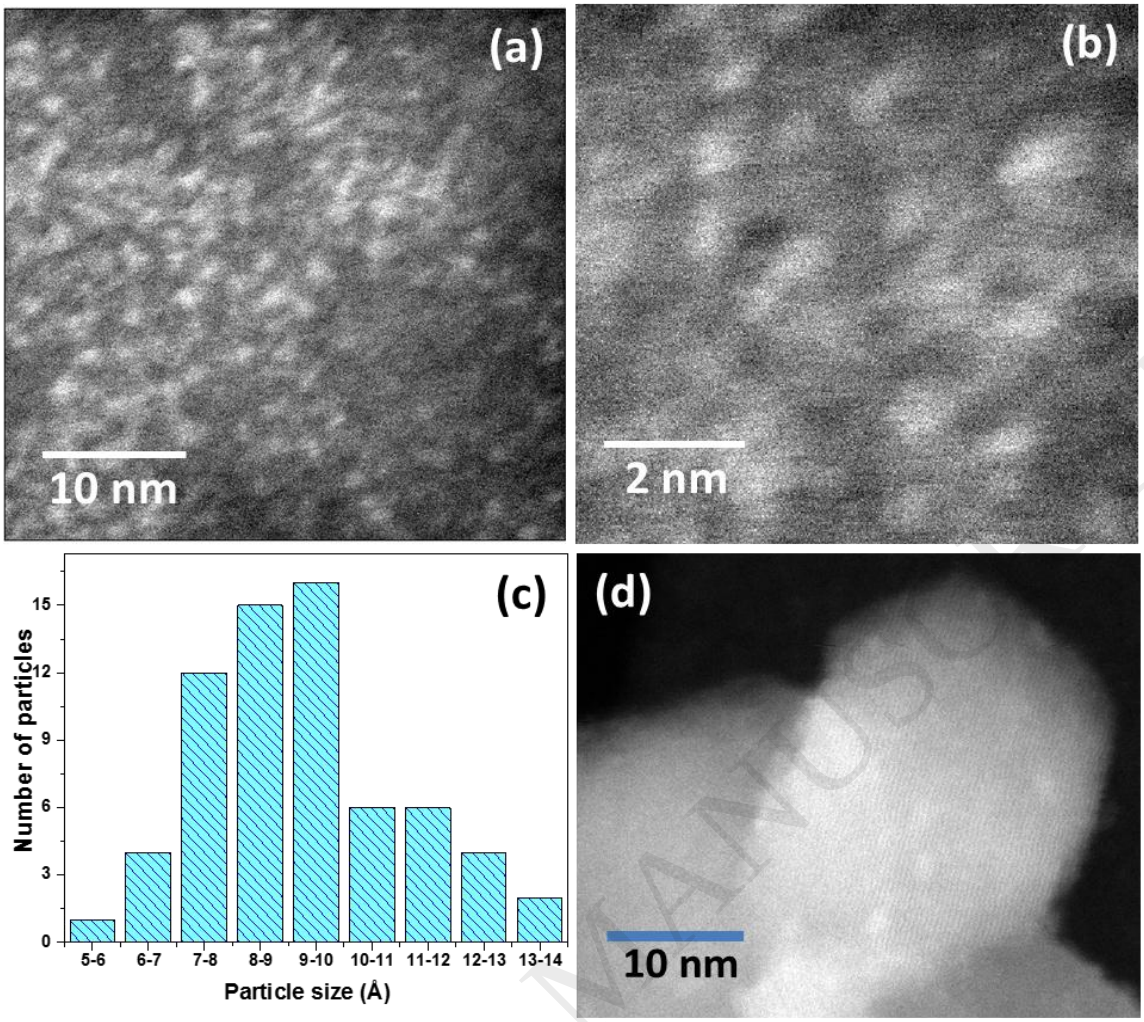

Figure 4. (a-b) STEM micrograph of unloaded Cu clusters, (c) corresponding particle size distribution of copper clusters and (d) STEM micrograph of Cu-P25.

The STEM image for Cu-TiO_2 post annealing is shown in figure 4(d). The P25 particle size measured from TEM is ~25 nm consistent with the manufacturer's data. The Cu clusters on the surface of titanium dioxide were observed in STEM mode as this provides enhanced surface contrast compared to TEM. Cu clusters, on the surface of P25 were observed with the mean size of ~9 Å which is comparable to the as-prepared cluster size. The slight increase in the copper particle size is believed to be an artefact due to the poor contrast of the edges of copper particles when observed on top of a TiO_2 background indicating that there is not marked increase in the cluster size following surface loading on titania and annealing. The distribution of Cu cluster sizes on P25 is shown in figure S6.

3.2 UV-Vis spectroscopy

The UV-Vis spectrum of copper clusters is given in Figure S2 with the MPP spectrum plotted for reference. Figure 5(a) shows the UV-Vis spectra of P25 before and after Cu modification. Surface modification of TiO_2 by CuO_x enhances the visible light absorption. The band-gap of P25 and Cu-P25 estimated from the Tauc plots (figure 5 (b)) are 3.02 and 2.83 eV,

respectively. This indicates a red-shift of 0.19 eV for the Cu-P25 as compared to the P25 alone. Indirect band gap estimation was utilised as this considers contributions from CuO_x. A similar sized red shift was observed when considering direct transition detailed in section S3 (figure S3).

Errors in determining the optical bandgap, using UV-Vis spectroscopy, apart from the absorption from non-interacting optical states modelling functions have a few assumptions which can affect the calculated value significantly. The Kubelka-Munk function ($F(R)=k/s=(1-R)^2/2R$, used for the Tauc plot) assumes that the thin film or sample is semi-infinite [40]. The bandgap value from Tauc plot depends on utilising the appropriate function to match the electronic transition present and on sufficient film thickness [41]. Given that our catalyst contains materials with both direct and indirect electronic transitions (for anatase and rutile components) neither fit can describe all states, leading to deviations from linearity in both treatments of optical data (figure 5(b) & S3(b)). The band gap determined from Tauc plots using direct and indirect transitions vary considerably (direct band-gap for P25 and Cu-P25 are 3.47 and 3.38 eV). Nevertheless, there is a red shift consistent with the predictions from the DFT simulations.

3.8 Spectral response

The current potential response under polychromatic UV-Vis and visible only irradiation is given in the supplementary information (Figure S7). The Cu-TiO_2 gave an enhanced UV-Vis photocurrent response as compared to the unmodified TiO_2 and a clear visible only response, with no significant photocurrent observed for the P25 ($\lambda > 435$ nm). The spectral photocurrent response of P25 and Cu-P25 were measured at fixed potential (+1.0 V) as illustrated in figure 6 (a and b). Surface modification with CuO_x gave a red shift in the UV response. Under visible light irradiation the unmodified P25 showed a small photocurrent response up to 410 nm, corresponding to the rutile band-gap of 3.0 eV, whereas the Cu-P25 gave a measurable photocurrent into the visible region (up to 500 nm, figure 6 (c)).

The spectral photocurrent response was used with light intensity measurements to obtain an incident photon to current efficiency (IPCE). Figure 7(a) shows that the IPCE was larger in the UV for the Cu-P25 as compared to the P25 alone. There is a clear red-shift of the IPCE for Cu-TiO_2, compared to P25, with a small tail into the visible region. The IPCE vs wavelength data were used for the Tauc like plots for the determination of the band gap [42]. A plot of $(IPCE*h\upsilon)^{1/2}$ as a function of photon energy in figure 7(b) gives indirect bandgaps of 2.96 eV (P25) and 2.85 eV (Cu-P25) with a small red-shift of 0.11 eV (16 nm).

4 Discussion

DFT simulation of CuO_x-TiO_2 predicts a reduction of the TiO_2 band gap due to the surface modification with CuO_x clusters, regardless of the TiO_2 polymorph. To test this prediction

experimentally, the band gap of copper cluster modified TiO_2 (P25) was measured using UV-Vis spectroscopy, XPS (valence band edge) and photoelectrochemical methods. In the UV-Vis measurement of the optical band gap, differentiating two overlapping absorbances from differing materials relies on using fits to existing models to identify two components being present. However, the use of Tauc plots, either $(F(R)h\upsilon)^2$ vs $h\upsilon$ or $(F(R)h\upsilon)^{1/2}$ vs $h\upsilon$ depending on direct or indirect transition, should lead to a straight line if only one component is present. Deviations from linearity observed in our measurements suggest that more than one transition was measured (anatase and rutile). As the films contain only 2 wt% of Cu as compared to TiO_2 it is very unlikely that the CuO_x signal alone would contribute, but rather it is due to states created by surface modification. Valence band XPS can also lead to overestimation of the red shift. Photocurrent measurements as a function of wavelength give the effective band gap. The p-type nature of CuO_x should result in a negligible contribution to photocurrent under positive bias. There is a smaller red shift in the photocurrent action spectrum as compared to diffuse reflectance and VB XPS. However, there is a clear red shift in the photocurrent action spectrum for the Cu-P25 as compared to the P25. This red shift is not due to Cu_2O because it is p-type semiconductor and should not give any anodic photocurrent under positive potential. The enhancement in the UV photocurrent is not due to oxidation of the Cu by the TiO_2 as the XPS analysis, following photoelectrochemical measurements, shows no change in the oxidation state, and the photocurrent is stable. The enhancement in the UV photocurrent cannot be due to electron transfer from the TiO_2 to the Cu_2O as the conduction band potential for the latter is more negative than that of the TiO_2 [43]. The visible photocurrent may be due to electron transfer from excited Cu_2O to the TiO_2 conduction band, however, that would likely lead to oxidation of the Cu(I) (which was not observed by XPS) and a decay in photocurrent over time. Examination of the IPCE data would suggest a red shift of effective band gap rather than any major enhancement of the UV response.

The experimental evidence correlates with the DFT predictions in that a red shift in the band gap of the Cu-TiO_2 is observed. While the red-shift in the band gap for the Cu-TiO_2 is not so marked, this work highlights a correlation between DFT simulations and actual experimental measurement of red shift in optical and photoelectrochemical response of CuO_x modified TiO_2.

5 Conclusions

DFT modelling predicts that small CuO_x nanoclusters, regardless of Cu oxidation state bind strongly to rutile and anatase surfaces and can produce states within the band gap of TiO_2 potentially narrowing the effective band gap. Characterisation of the as-prepared copper clusters indicated that size controlled could be achieved using a modified Brust-Schiffrin method. The conditions of loading and thermal processing of these clusters on titania was observed to maintain particle size and oxidation state of the copper clusters. The influence of copper modification on the band gap of P25 was investigated by looking at changes to the

optical absorbance, VB region XPS and by photoelectrochemical methods. Surface modification of the TiO_2 with CuO_x clusters did give a red shift of the optical band gap of ~0.2 eV. Extrapolation of the valence band edge in XPS showed a reduction in band gap of nearly 0.6 eV. Extrapolation of IPCE data with respect to wavelength suggest much smaller changes to the effective band gap of the material (0.11 eV). This work highlights the enormous potential for computational design to discover new photocatalytic materials that may be useful for solar applications

Acknowledgements

The authors acknowledge support from the US-Ireland R&D Partnership Program, NSF (CBET-1438721), SFI (SFI 14/US/E2915) and DfE (USI065). We also acknowledge Ulster University for funding the PhD scholarship for PKS and Invest Northern Ireland for funding (RD0713920). Computing resources at Tyndall are supported by SFI and at the SFI and Higher Education Authority funded Irish Centre for High End Computing.

References

References

[1] A. Fujishima, X. Zhang, D.A. Tryk, Surf. Sci. Rep. 63 (2008) 515-582.

[2] A. Kudo, Y. Miseki, Chem. Soc. Rev. 38 (2009) 253-278.

[3] D.A. Tryk, A. Fujishima, K. Honda, Electrochim. Acta 45 (2000) 2363-2376.

[4] J.W.J. Hamilton, J.A. Byrne, C. McCullagh, P.S.M. Dunlop, Int. J. Photoenergy article ID 631597 (2008) 8 pages.

[5] S. Baskoutas, A.F. Terzisa, J. Appl. Phys. 99 (2006) 013708.

[6] G.W. Luther, D.T. Rickard, S. Theberge, A. Olroyd, Environ. Sci. Technol. 30 (1996) 671–679.

[7] G. Kim, Y. Park, G.-h. Moon, W. Choi, Photoexcitation in Pure and Modified Semiconductor Photocatalysts, in: J. Schneider, D. Bahnemann, J. Ye, G.L. Puma, D.D. Dionysiou (Eds.), Photocatalysis: Fundamentals and Perspectives, RSC, Cambridge, 2016, pp. 110-128.

[8] M. Abdulla-Al-Mamun, Y. Kusumoto, G.J. Islam, J. Sci. Res. 5 (2013) 245-254.

[9] H. Tada, Q. Jin, A. Iwaszuk, M. Nolan, J. Phys. Chem. C. 118 (2014) 12077–12086.

[10] A. Iwaszuk, M. Nolan, Q. Jin, M. Fujishima, and H. Tada J. Phys. Chem. C. 117 (2013) 2709-2718

[11] A. Iwaszuk, M. Nolan, J. Mater. Chem. A. 1 (2013), 6670-6677

[12] M. Nolan, A. Iwaszuk, A. K. Lucid, J. J. Carey, M. Fronzi, Adv. Mater. 28 (2016) 5425–5446.

[13] M. Fronzi, A. Iwaszuk, A. Lucid and M. Nolan J. Phys. Condens. Matter, 28, (2016) art. 074006

[14] A. Iwaszuk, M. Nolan, Phys. Chem. Chem. Phys. 13 (2011) 4963

[15] M. Fronzi, W. Daly, M. Nolan, Appl. Catal. A 521 (2016) 240

[16] P.V. Kamat, J. Phys. Chem. Lett. 3 (2012) 663−672.

[17] A. Reynal, F. Lakadamyali, M.A. Gross, E. Reisner, J.R. Durrant, Energy Environ. Sci. 6 (2013) 3291-3300.

[18] M. Nolan, A. Iwaszuk, K.A. Gray J. Phys. Chem. C. 118 (2014) 27890-27900

[19] A. Iwaszuk, A.K. Lucid, K.M. Razeeb M. Nolan J. Mater. Chem. A, 2, (2014) 18796-18805

[20] S. Linic, P. Christopher, D.B. Ingram, Nat. Mater. 10 (2011) 911−921.

[21] C.G. Silva, R. Juarez, T. Marino, R. Molinari and H. Garcia, J. Am. Chem. Soc. 133 (2011) 595–602.

[22] P. de Jongh, D. Vanmaekelbergh J. Kelly, Chem. Commun., 12 (1999), 1069-1070.

[23] Y. Jiang, H. Yuan, and H. Chen, Phys. Chem. Chem. Phys. 17 (2015) 630-637.

[24] Z. Wang, Y. Liu, D. J. Martin, W. Wang, J. Tang and W. Huang, Phys. Chem. Chem. Phys. 15 (2013) 14956–14960.

[25] J. P. Yasomanee and J. Bandara, Sol. Energ. Mat. Sol. Cells 92 (2008) 348–52.

[26] Z. Wang, D. Brouri, S. Casale, L. Delannoy and C. Louis, J. Catal. 340 (2016) 95–106.

[27] Q. Jin, M. Fujishima, A. Iwaszuk, M. Nolan, H. Tada, J. Phys. Chem. C 117 (2013), 23848-23857

[28] N. Seriani, C. Pinilla and Y. Crespo, J. Phys. Chem. C 119 (2015) 6696−6702.

[29] G. Kresse, and J. Furthmüller, Comp. Mater. Sci. 6 (1996) 15-50.

[30] G. Kresse, J. Furthmüller, Phys. Rev. B, 54 (1996) 1116954,

[31] W. Wei, Y. Lu, W. Chen, S. Chen, J. Am. Chem. Soc. 133 (2011) 2060–2063.

[32] J.A. Byrne, B.R. Eggins, N.M.D. Brown, B. McKinney, M. Rouse, Appl. Catal. B 17 (1998) 25-36.

[33] A. Iwaszuk, M. Nolan, Catal. Sci. Technol. 3, (2013) 2000.

[34] V.B.R. Boppana, F. Jiao, D. Newby, J. Laverock, K.E. Smith, J.C. Jumas, G. Hutchings, R.F.Lobo, Phys. Chem. Chem. Phys. 15 (2013), 6185

[35] D.S. Bhachu, S. Sathasivam, C.J. Carmalt, I.P. Parkin, Langmuir 30 (2014), 624.

[36] C.D. Wagner, A.V. Naumkin, A. Kraut-Vass, J.W. Allison, C.J. Powell, J.R. Jr. Rumble, NIST Standard Reference Database 20, Version 3.4 (web version) 2003.

[37] M.C. Biesinger, L.W.M. Lau, A.R. Gerson, R.St.C. Smart, Appl. Surf. Sci. 257 (2010) 887-898.

[38] D. Kim, S. Lee, J.D. Ocon, B. Jeong, J.K. Lee, J. Lee, Phys. Chem. Chem. Phys. 17 (2015) 824-830.

[39] K. Jayaramulu, T. Toyao, V. Ranc, C. Rösler, M. Petr, R. Zboril, Y. Horiuchi, M. Matsuoka, R.A. Fischer, J. Mater. Chem. A 4 (2016) 18037-18042.

[40] A.A. Kokhanovsky, J. Phys. D: Appl. Phys. 40 (2007) 2210–2216

[41] M.E. Sánchez-Vergara, J.C. Alonso-Huitron, A. Rodriguez-Gómez, J.N. Reider-Burstin, Molecules 17 (2012) 10000-10013.

[42] A. Mazare, I. Paramasivam, F. Schmidt-Stein, K. Lee, I. Demetrescu, P. Schmuki, *Electrochim. Acta,* 66 (2012), 12–21.

[43] A. Paracchino, V. Laporte, K. Sivula, M. Grätzel and E. Thimsen, Nat. Mater., 10, (2011), 456–461

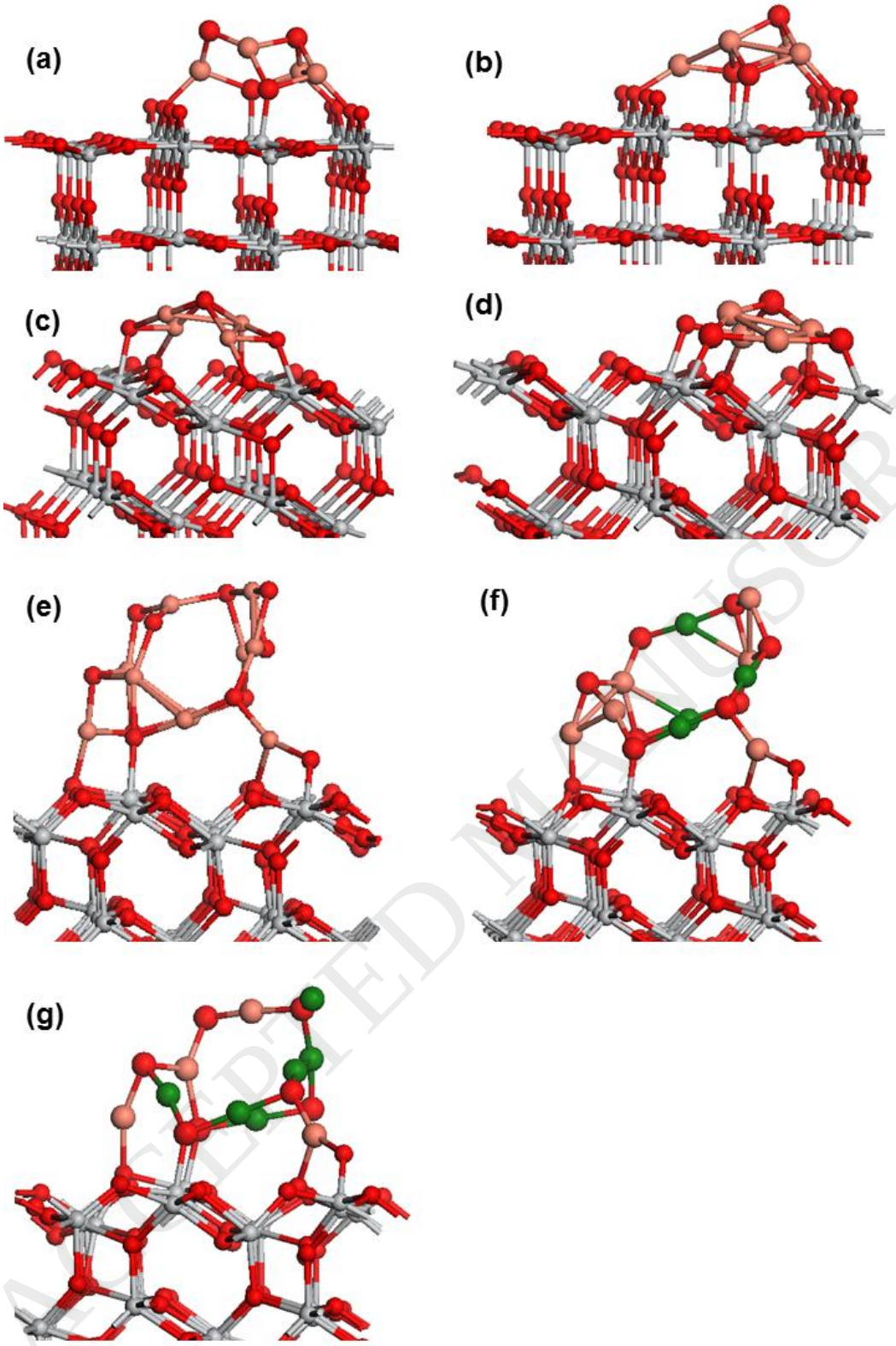

Figure 1. *Atomic structure of CuO nanocluster modified TiO_2.* ***(a), (b):*** *Cu_4O_4 and Cu_4O_3-modified rutile (110)* ***(c) (d)*** *Cu_4O_4 and Cu_4O_3-modified anatase (101)* ***(e)*** *$Cu_{10}O_{10}$-modified anatase (101),* ***(f)*** *$Cu_{10}O_8$-modified anatase (101) with two oxygen vacancies, the ground state and* ***(g)*** *$Cu_{10}O_7$-modified anatase (101), with three oxygen vacancies, after forming a reducing*

oxygen vacancy. Ti atoms are grey spheres, O atoms are red, Cu atoms are salmon spheres. Green spheres in parts (f) and (g) show Cu^{+} sites.

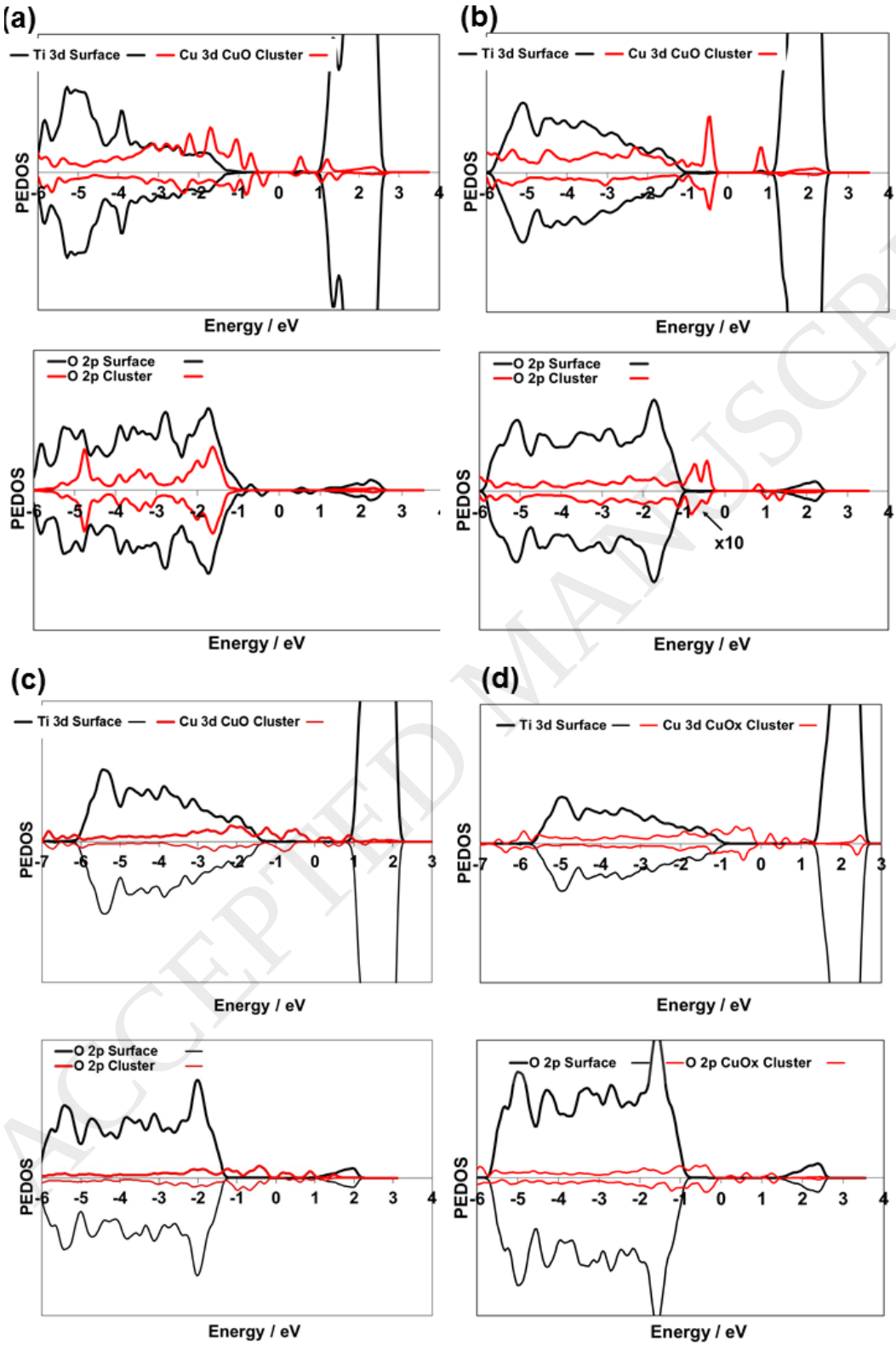

Figure 2. Spin polarised projected electronic density of states (PEDOS) projected onto Cu and Ti 3d states (top panels) and O 2p states (bottom panels) in the anatase surface and the

CuO nanocluster. **(a)** Cu_4O_4-modified rutile (110), **(b)** Cu_4O_4-modified anatase (101), **(c)** $Cu_{10}O_{10}$-modified anatase (101) and **(d)** $Cu_{10}O_8$-modified anatase (101), the stable ground state. The zero of energy is the Fermi level.

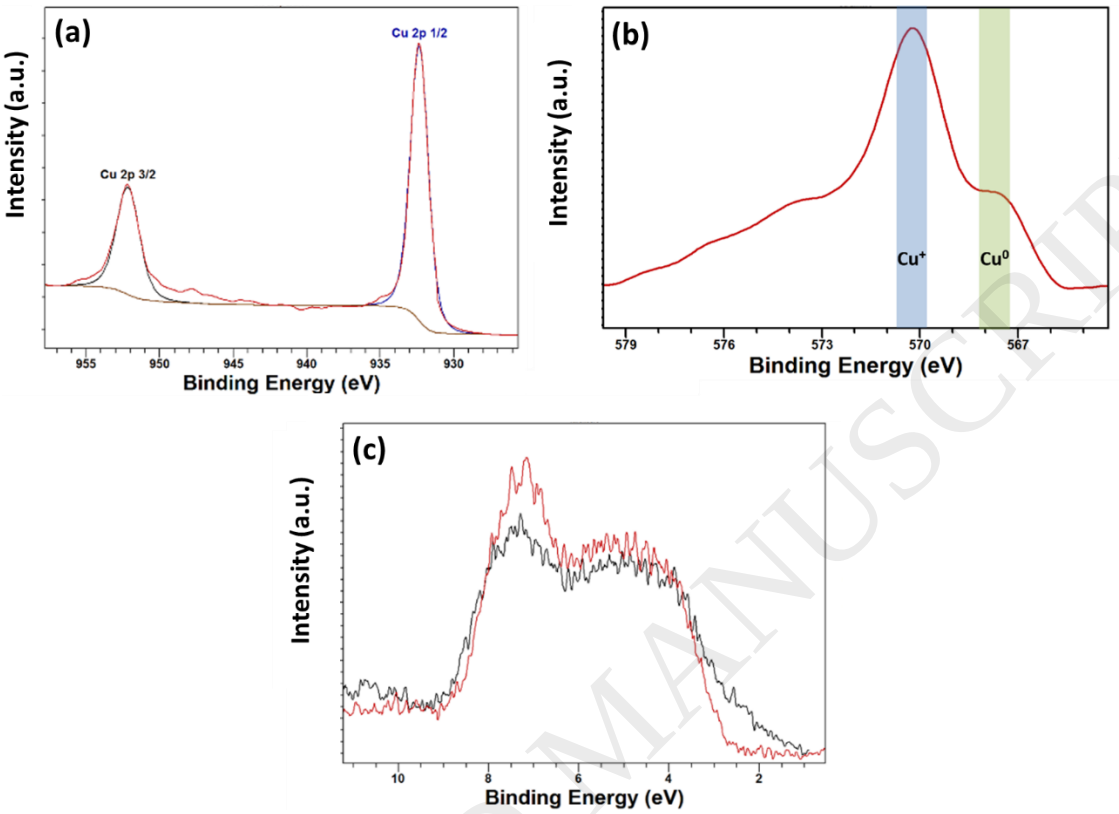

Figure 3. (a) Cu 2p, (b) Cu LMM XPS spectra of the as-prepared copper clusters, and (c) valence band XPS for P25 (red lines) and Cu-P25 (black lines) samples.

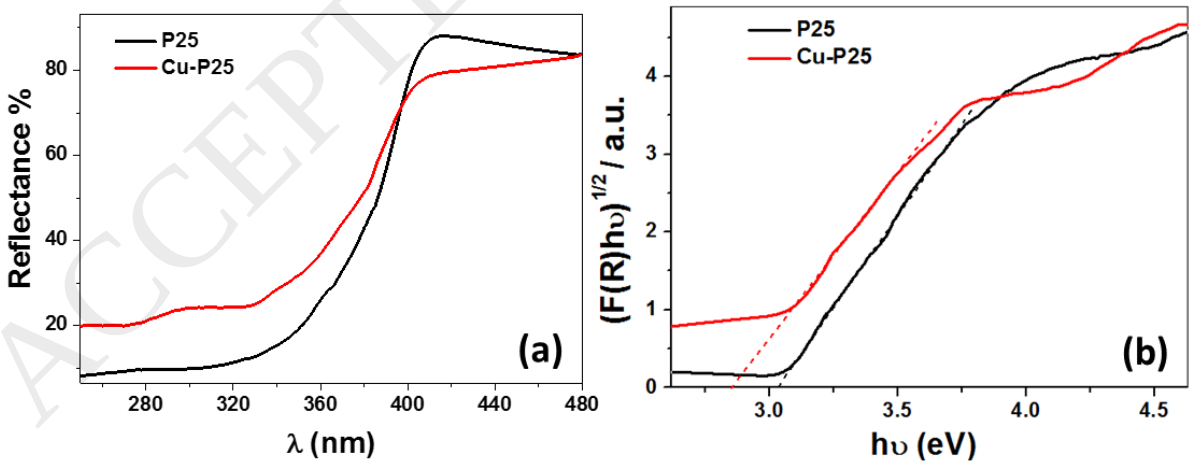

Figure 5. (a) UV-Vis reflectance spectra for P25 and Cu-P25 annealed at 550°C and (b) corresponding Tauc plot considering an indirect band-gap.

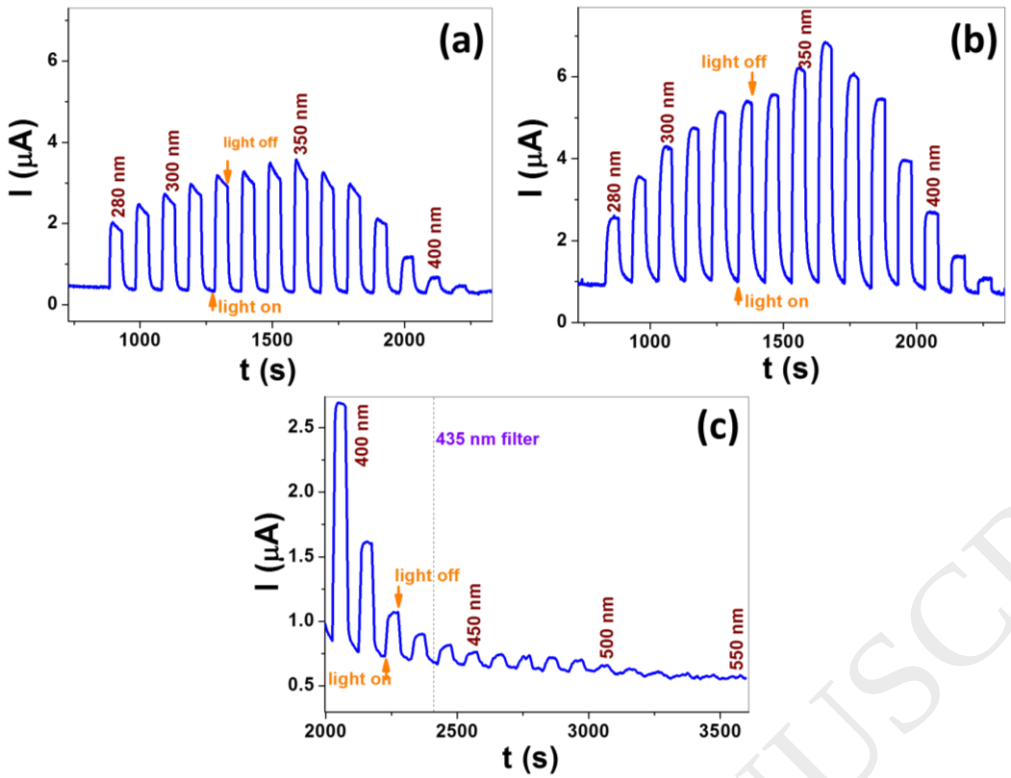

Figure 6. Spectral response of (a) P25 and (b) Cu-P25 and, (c) Cu-P25 in visible region only. The figures show the current vs time with light on and off, increasing the monochromatic wavelength in each measurement by 10 nm. The wavelength of irradiation is given as the number above the photocurrent. The UV cut-off filter (435 nm) was used after the 430 nm measurement. Electrolyte 0.1 M $HClO_4$, +1.0 V vs. SCE, 10 nm interval, 50 s exposure-delay cycle.

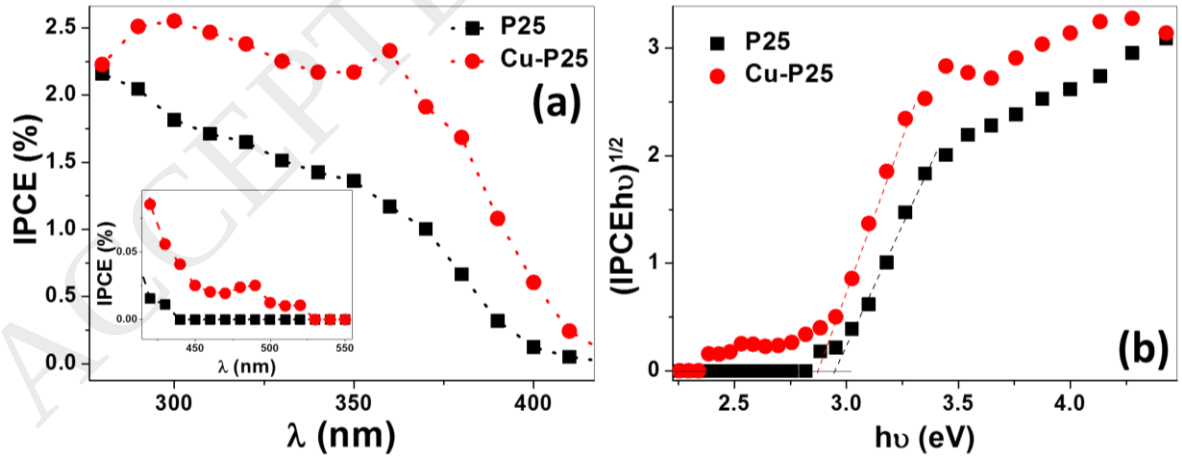

Figure 7. Combined IPCE plots of P25 and Cu-P25 samples, the inset shows the response in visible region and (e) Tauc plot from IPCE considering the indirect band-gap materials.